석사 학위논문

Master Thesis

층간 슬립을 고려한 적층 쉘 유한요소 개발

Development of the layered shell finite element with interlayer slip

2021

이 준 호 (李 俊 互 Lee, June Ho)

한 국 과 학 기 술 원

Korea Advanced Institute of Science and Technology

석 사 학 위 논 문

층간 슬립을 고려한 적층 쉘 유한요소 개발

2021

이 준 호

한 국 과 학 기 술 원

기계항공공학부/기계공학과

층간 슬립을 고려한 적층 쉘 유한요소 개발

이 준 호

위 논문은 한국과학기술원 석사학위논문으로
학위논문 심사위원회의 심사를 통과하였음

2020년 12월 4일

심사위원장 이 필 승 (인)
심 사 위 원 김 성 수 (인)
심 사 위 원 유 승 화 (인)

Development of the layered shell finite element with interlayer slip

Lee, June Ho

Advisor: Phill-Seung Lee

A dissertation submitted to the faculty of
Korea Advanced Institute of Science and Technology in
partial fulfillment of the requirements for the degree of
Master of Science in Mechanical Engineering

Daejeon, Korea
December 4, 2020

Approved by

Phill-Seung Lee
Professor of Mechanical Engineering

The study was conducted in accordance with Code of Research Ethics[1)].

1) Declaration of Ethical Conduct in Research: I, as a graduate student of Korea Advanced Institute of Science and Technology, hereby declare that I have not committed any act that may damage the credibility of my research. This includes, but is not limited to, falsification, thesis written by someone else, distortion of research findings, and plagiarism. I confirm that my dissertation contains honest conclusions based on my own careful research under the guidance of my advisor.

MME 이준호. 층간 슬립을 고려한 적층 쉘 유한요소 개발. 기계공학과. 2020년. 37+iii 쪽. 지도교수: 이필승. (영문 논문)
Lee, Juneho. Development of the layered shell finite element with interlayer slip. Department of Mechanical Engineering. 2020. 37+vii pages. Advisor: Lee, Phill-Seung. (Text in English)

초 록

본 학위 논문에서는 적층 구조물의 층간 부분 상호 작용을 고려한 유한요소 해석을 위해 층간 슬립을 고려한 새로운 적층 쉘 요소를 제안한다. 제안하는 적층 쉘 요소는 추가적인 쉘을 이용하여 층을 모델링하지 않고 슬립 방향으로의 자유도만 추가함에 따라 계산에 필요한 자유도 수를 줄여 해석의 효율성을 크게 향상시킨다. 기존의 층간 슬립을 고려한 요소는 솔리드 요소나 빔 요소로 제한되어 있으며 얇은 재료들을 해석할 때 필요한 자유도수가 매우 증가하거나 2차원 부분 상호작용을 고려하지 못한다는 단점이 존재하였다. 하지만 본 기법에서는 이차원 슬립 평면에서 슬립이 일어나는 방향을 정의하여 각 노드당 두개의 추가적인 자유도로 적층을 표현할 수 있다. 또한 정의된 두 개의 슬립 방향을 이용하여 층 사이의 2차원 부분 상호작용도 고려 가능하다. 제안한 쉘 모델의 성능을 확인하기 위해 다양한 수치 예제를 통해 비교한 결과 접착층을 고려한 솔리드 요소를 사용하는 것에 비해 높은 계산 효율성을 가지고 정확한 유한 요소 해석이 가능하다는 것을 확인하였다. 본 선형 요소를 비선형 요소 식으로 확장한다면 변형이 증가함에도 보다 정확한 해석이 가능할 것이라 기대한다.

핵심낱말 유한요소법, 복합 쉘 모델, 다층 쉘 요소, 층간 슬립, 부분상호작용

Abstract

A finite element analysis using a new layered shell element considering the partial interaction of the layers has been proposed. The proposed layered shell element improves the efficiency of analysis by adding only the DOFs in the slip direction without modeling the layers using additional shells. Existing elements that attempted interlayer slip were limited to solid elements or beam elements, and there were disadvantages in that the DOFs required when analyzing thin materials was increased or that two-dimensional partial interactions were not considered. Unlike with previous element, the stacking can be expressed with two additional DOFs per node by defining the direction in which the slip occurs in the two-dimensional slip plane. 2D interlayer slip between layers can also be considered using the defined slip directions. As a result of comparing through several numerical examples it was confirmed that accurate finite element analysis is possible with high computational efficiency compared to using the solid element considering the adhesive layer. If this linear shell is extended to a nonlinear formulation, it is expected that more accurate analysis will be possible even through the deformation increase.

Keywords finite element method, composite shell, multi-layered shell, interlayer slip, partial interaction

Contents

List of Tables

List of Figures

Chapter 1. Introduction

As the machinery industry evolves, FEM analysis, which reduces design costs and increases design accuracy, has also evolved. As a result, FEM analysis is widely used not only in the mechanical field, but also in the aviation, construction and even the bio field such as bone tissue engineering. However, with the form factor innovation that deviated from the existing rigid form factor, the new FEM analysis element was needed. Foldable mobile phones and rollable TVs are examples of typical form factor innovations. In the case of such an item, a thin composite was used and there is an adhesive layer between the materials, so it is not easy to proceed with the analysis in the traditional way.

In the case of conventional composite research, Classical Lamination Theories CLT, a laminated plate with completely bonded layers, was presented by Reissner and Stavwsky [1]. To improve the problem caused by not considering the transverse shear strain, First order Shear Deformation Theory FSDT was introduced by Yang, Norris and Stavsky [2]. Two-layer plate analysis considering slip, which is discontinuity between layers, is proposed by Toledano and Murakami [3]. Trial displacement in which the zigzag term considering the shear strain and slip displacement term were superposed to the existing plate theory was used for the two-layer plate analysis. Afterwards, a theory that considered interlayer slip in multilayer plates was proposed by Marco Di Sciuva [4].

Composite materials were studied not only for the previously described plate but also for beam and shell elements. Like the plate, it started with a two-layer and expanded into a multi-layer. Newmark suggested a two-layer beam with interlayer slip added to Euler Bernoulli's beam theory [5]. After that, Xu and Wu implemented interlayer slip using Timoshenko beam theory considering shear deformation [6].

Furthermore, a finite element algorithm for a composite beam with interlayer slip was implemented by Ranzi et al [7]. Most recently, a continuum-based nonlinear layered composite beam element with interlayer slip was presented by Hyo-Jin Kim [8]. However, it is not suitable for analyzing thin and wide structures with beam elements. Laminated composite shell elements using finite elements suitable for thin structure analysis were proposed by Panda and Natarajan [9], but interlayer slip was not considered. There is a need for research on laminated composite shell elements in which partial interactions exist.

Compared to a beam with partial interaction in only one direction in an interlayer, the shell slips in two directions, which requires more complex structural behavior. Because of such difficulties, it is not easy to find a laminated composite shell FE model in which layer partial interaction occurs. In the case of existing commercial analysis tools, solid elements are used to solve the problem. But in the case of thin structures, the number of elements rapidly increases for accurate analysis.

The purpose of this study is to develop a layered composite shell element that considers slip in the interlayer by using fewer elements even when analyzing thin structures. First, the layers are divided from the basic shell elements, and then a degree of freedom is added for each layer to consider the displacement discontinuity due to partial interaction. Analysis can be performed using fewer elements than modeling all layers.

In Chapter 2, a brief review of finite element analysis of basic shell structures will be conducted. And then, the continuum mechanism based layered composite shell element that the interlayer slip did not consider [9] will be covered in more detail.

In Chapter 3, the proposed shell element considering interlayer slip will be explained. First, displacement interpolation is defined, and then the finite element discretization process will be examined.

In Chapter 4, various numerical examples are presented to verify the proposed shell elements.

In Chapter 5, the conclusions of this study and future studies will be described.

Chapter 2. Review of 4-node continuum mechanics based shell finite elements

In this chapter, the theory of three-dimensional continuum mechanics was examined. First, the displacement interpolation of a general 4-node shell element was presented [10]. This displacement interpolation poses a problem that causes transverse shear locking. Therefore, the MITC4 method was reviewed to solve this problem [11]. Finally, the displacement interpolation extended to the laminated shell element was presented [9].

2.1. Displacement Interpolation

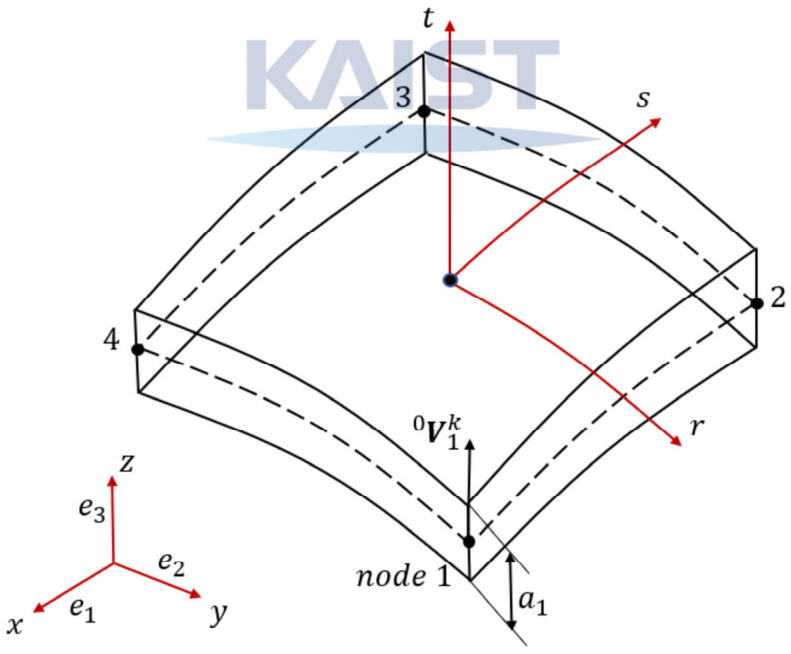

Fig. 2.1. Geometry of 4-node shell elements

Consider the geometry of the 4-node shell elements in Fig. 2.1. Using the natural coordinate system r, s and t, the geometry interpolation for any point in the 4-node shell element at a given time t is obtained by

$$ {}^{t}\boldsymbol{x}(r,s,t) = \sum_{k=1}^{4} h_k(r,s)\,{}^{t}\boldsymbol{x}_k + \frac{t}{2}\sum_{k=1}^{4} a_k h_k(r,s)\,{}^{t}\boldsymbol{V}_n^k \ , \tag{2.1} $$

where h_k is the 2D interpolation function at node k, ${}^{t}\boldsymbol{x}_k$ is Cartesian coordinates of the node k at time t, a_k is thickness of shell of node k, ${}^{t}\boldsymbol{V}_n^k$ denotes the direction vector defined of node k at time t and the left superscript t is the configuration of the shell element at given time t. $t=0$ denotes the original configuration, so the displacement interpolation of the element for the configuration at time t is obtained as by using Eqs. (2.1).

$$ {}^{t}\boldsymbol{u} = {}^{t}\boldsymbol{x} - {}^{0}x \ , \tag{2.2} $$

$$ {}^{t}\boldsymbol{u}(r,s,t) = \sum_{k=1}^{4} h_k(r,s)\,{}^{t}\boldsymbol{u}_k + \frac{t}{2}\sum_{k=1}^{4} a_k h_k(r,s)({}^{t}\boldsymbol{V}_n^k - {}^{0}\boldsymbol{V}_n^k) \ , \tag{2.3} $$

where ${}^{t}\boldsymbol{u}_k$ is the vector of nodal displacements in the Cartesian coordinate direction and ${}^{0}\boldsymbol{V}_n^k$ denotes the direction vector defined of node k in the reference configuration. ${}^{0}\boldsymbol{V}_1^k$ and ${}^{0}\boldsymbol{V}_2^k$ are orthogonal to ${}^{0}\boldsymbol{V}_n^k$ in the configuration at time 0 are defined as (See Fig. 2.2.)

$$ {}^{0}\boldsymbol{V}_1^k = \frac{\boldsymbol{e}_2 \times {}^{0}\boldsymbol{V}_n^k}{\left|\boldsymbol{e}_2 \times {}^{0}\boldsymbol{V}_n^k\right|} \ , \tag{2.4} $$

$$ {}^{0}\boldsymbol{V}_2^k = {}^{0}\boldsymbol{V}_n^k \times {}^{0}\boldsymbol{V}_1^k \ , \tag{2.5} $$

where $\boldsymbol{e}_2$ is a unit vector in the y-axis direction.

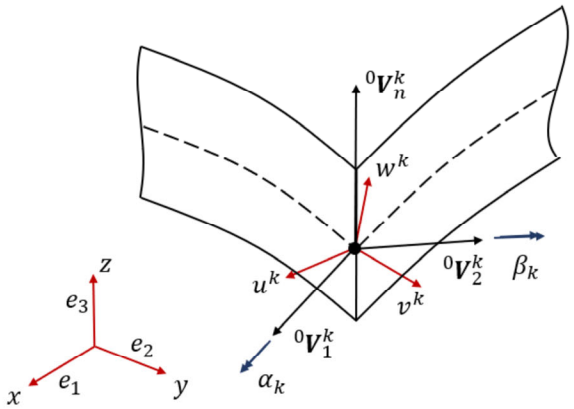

Fig. 2.2. Rotational DOF α_k and β_k at node k

Using the rotational DOF α_k and β_k of the vectors ${}^0\boldsymbol{V}_1^k$ and ${}^0\boldsymbol{V}_2^k$, the direction vector of node k at time t with infinitesimal rotations can be expressed as

$$ {}^t\boldsymbol{u}(r,s,t) = \sum_{k=1}^{4} h_k(r,s)\,{}^t\boldsymbol{u}_k + \frac{t}{2}\sum_{k=1}^{4} a_k h_k(r,s)(-\alpha_k\,{}^0\boldsymbol{V}_2^k + \beta_k\,{}^0\boldsymbol{V}_1^k)\ . \tag{2.6} $$

Then the covariant Green-Lagrange strain tensor components are

$$ {}^t_0\tilde{\varepsilon}_{ij} = \frac{1}{2}({}^t\boldsymbol{g}_i\,{}^t\boldsymbol{g}_j - {}^0\boldsymbol{g}_i\,{}^0\boldsymbol{g}_j),\quad {}^t\boldsymbol{g}_i = \frac{\partial {}^t\boldsymbol{x}}{\partial r_i}\ , \tag{2.7} $$

where ${}^t g_i$ is the covariant base vector with i = 1, 2, 3 corresponding to $r_1 = r$, $r_2 = s$, $r_3 = t$

2.2. Formulation of the MITC4 method

The above interpolation causes a locking phenomenon that reduces the convergence rate of finite element analysis for thin elements. Many methods have been used to alleviate this transverse shear locking phenomenon. Among them, MITC4, which is a method of introducing a separate interpolation in the transverse shear strain, was described [10]

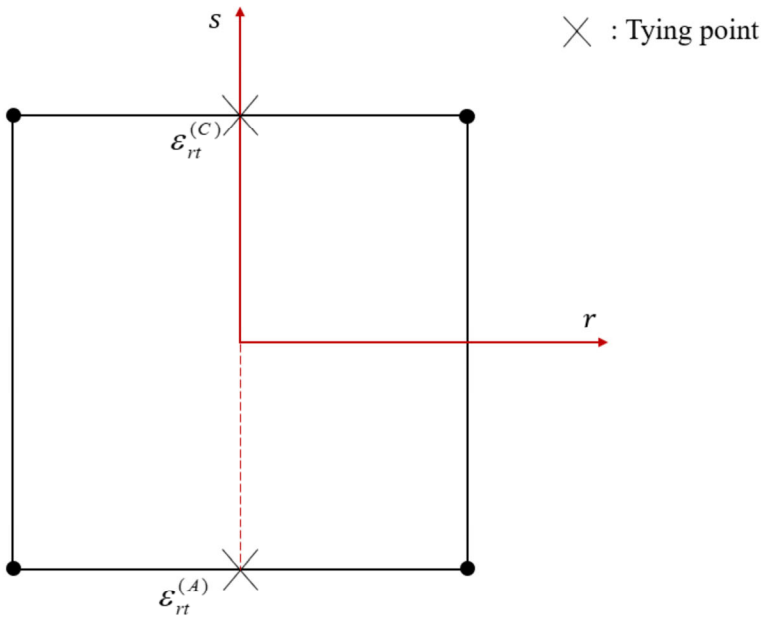

(a)

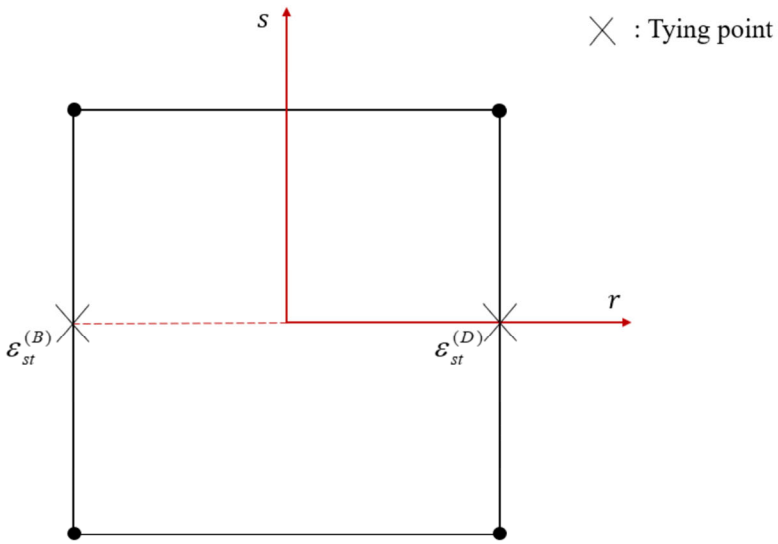

(b)

Fig. 2.3. Tying points for the 4-node shell finite elements in MITC4 (a) assumed strain in $r-t$ (b) assumed strain in $s-t$

It is assumed that the tying position given in Fig. 2.3 constructs a constant deformation along the upper and lower edges of the element. Hence, the assumed transverse shear strain fields using the interpolation and tying points of the MITC4 are written by:

$$\varepsilon_{rt}^{AS} = a_{rt} + b_{rt}r + c_{rt}s + d_{rt}rs \tag{2.8}$$

and

$$\varepsilon_{st}^{AS} = a_{st} + b_{st}r + c_{st}s + d_{st}rs \ . \tag{2.9}$$

where $a_{rt} = \frac{1}{2}(\varepsilon_{rt}^{(A)} + \varepsilon_{rt}^{(C)})$, $c_{rt} = \frac{1}{2}(\varepsilon_{rt}^{(C)} - \varepsilon_{rt}^{(A)})$, $b_{rt} = d_{rt} = 0$, $a_{st} = \frac{1}{2}(\varepsilon_{st}^{(B)} + \varepsilon_{st}^{(D)})$,

$b_{st} = \frac{1}{2}(\varepsilon_{st}^{(D)} - \varepsilon_{st}^{(B)})$, $c_{st} = d_{st} = 0$.

2.3. **Layered shell displacement interpolation**

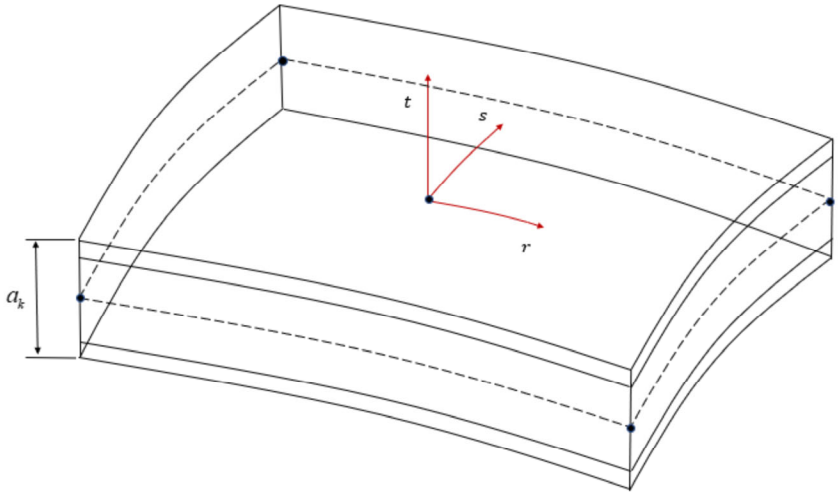

Fig. 2.4. Geometry of layered shell elements

In the case of laminated materials, as shown in Fig. 2.4, different material properties of the layer must be considered. Therefore, it is necessary to add by performing numerical integration of the stiffness matrix for each layer. In order to perform numerical integration by dividing, a new natural coordinate system according to the thickness of the element must be used. The new natural coordinate of nth layer t^n is derived as

$$t = -1 + \frac{1}{a_k}\left\{2\left(\sum_{i=1}^{n} l^i\right) - l^n(1-t^n)\right\}, \tag{2.10}$$

where t is original natural coordinate, a_k is total thickness of shell at node k, l^n is thickness of nth layer.

Substituting Eqs. (2.10) into Eqs. (2.1), the geometry interpolation of nth layer is given as

$$\boldsymbol{x}^{(n)} = \sum_{k=1}^{4} h_k \boldsymbol{x}_k^{(n)} + \sum_{k=1}^{4}\left(m_k^{(n)} + \frac{l_k^{(n)}}{2} t^{(n)}\right) h_k \boldsymbol{V}_n^k, \tag{2.11}$$

where $m_k^{(n)}$ is distance between the midsurface of layer n and the total element midsurface at node k.

The formulation of $m_k^{(n)}$ obtained using Fig. 2.5

$$m_k^{(n)} = -\frac{a_k}{2} + \sum_{i=1}^{n} l_k^{(i)} - \frac{l_k^{(n)}}{2} \,. \tag{2.12}$$

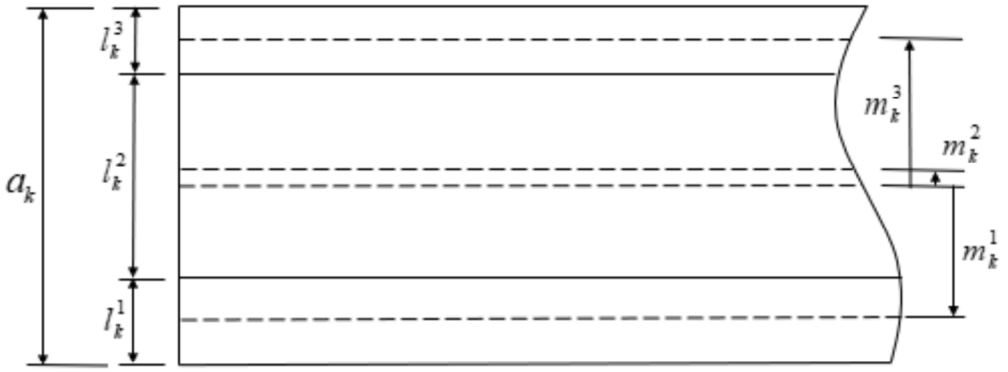

Fig. 2.5. Thickness and midsurface position of layer n

Using geometry interpolation, the displacement interpolation of layer n is obtained as

$$\boldsymbol{u}^{(n)} = \sum_{k=1}^{4} h_k \boldsymbol{u}_k^{(n)} + \sum_{k=1}^{4} \left(m_k^{(n)} + \frac{l_k^{(n)}}{2} t^{(n)} \right) h_k (-\alpha_k {}^0\boldsymbol{V}_2^k + \beta_k {}^0\boldsymbol{V}_1^k) \,. \tag{2.13}$$

The linear component in Green-Lagrange strain of Equation 2.8 in layer n is given by

$${}_0^t\tilde{e}_{ij}^{(n)} = \frac{1}{2}({}^t\boldsymbol{g}_i^{(n)} \frac{\partial_0 \boldsymbol{u}^{(n)}}{\partial r_j} + {}^t\boldsymbol{g}_j^{(n)} \frac{\partial_0 \boldsymbol{u}^{(n)}}{\partial r_i}) \,, \quad {}^t\boldsymbol{g}_i^{(n)} = \frac{\partial {}^t\boldsymbol{x}^{(n)}}{\partial r_i} \,, \tag{2.14}$$

where r_i is natural coordinate corresponding to $r_1 = r$, $r_2 = s$, $r_3 = t^{(n)}$.

Using coordinate transformation, the Green-Lagrange strain in the local Cartesian coordinate system is obtained as

$${}_0^t\bar{e}_{ij}^{(n)} = (\hat{\boldsymbol{e}}_i \cdot {}^0\boldsymbol{g}^{k(n)})(\hat{\boldsymbol{e}}_j \cdot {}^0\boldsymbol{g}^{l(n)}) {}_0\tilde{e}_{kl}^{(n)} \,, \tag{2.15}$$

where $\hat{\boldsymbol{e}}_i$ is local Cartesian coordinate, ${}^0\boldsymbol{g}^{k(n)}$ is covariant base vector in layer n.

The local Cartesian coordinate system is defined as:

$$\hat{\boldsymbol{e}}_3 = \frac{\boldsymbol{g}_3^{(n)}}{\left|\boldsymbol{g}_3^{(n)}\right|} \quad , \tag{2.16}$$

$$\hat{\boldsymbol{e}}_1 = \frac{\boldsymbol{g}_2^{(n)} \times \hat{\boldsymbol{e}}_3}{\left|\boldsymbol{g}_2^{(n)} \times \hat{\boldsymbol{e}}_3\right|} \quad , \tag{2.17}$$

$$\hat{\boldsymbol{e}}_2 = \hat{\boldsymbol{e}}_3 \times \hat{\boldsymbol{e}}_1 \quad . \tag{2.18}$$

For finite element discretization, the strain-displacement matrix B is obtained as

$${}_0^t\overline{\varepsilon}_{ij}^{(n)} = \overline{\boldsymbol{B}}_{ij}\boldsymbol{U} \quad , \tag{2.19}$$

with

$$\boldsymbol{U} = [u_1 \;\; u_2 \;\; \ldots \;\; u_4 \;\; v_1 \;\; \ldots \;\; w_1 \;\; \ldots \;\; \alpha_1 \;\; \ldots \;\; \beta_1 \;\; \ldots \;\; \beta_4]^T .$$

From the $\boldsymbol{U}$ of Eqs. (2.19), it can be seen that the slip of each layer cannot be expressed in the degree of freedom of the layered shell element.

Chapter 3. Continuum mechanics based shell element with interlayer slip

In this chapter, three-dimensional continuum mechanics based shell element formulation considering slip is derived. was examined. In the case of the shell, since two-dimensional partial interaction occurs in the interlayer, the slip is defined using two direction vectors. Thereafter the degree of freedom of each layer added for geometry interpolate was described. The finite element analysis of this shell element is explained by applying the principle of virtual work, and the discretization process is summarized.

3.1. Displacement Interpolation

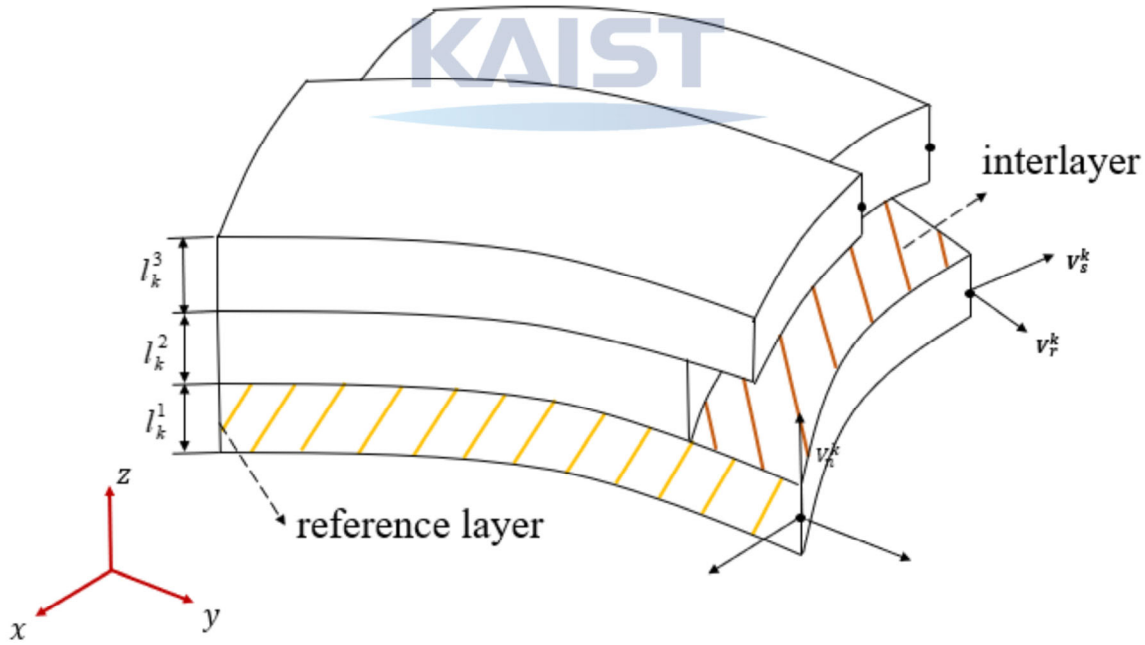

Fig. 3.1. Geometry of 4-node shell element with interlayer slip

Eqs. (2.13) in Chapter 2, a shell element based on continuum mechanics without slip consideration was introduced. In order to account for slip in the laminated shell element, the displacement discontinuity of each layer must be considered. In Fig. 3.1, a single shell element consists of several layers. Slip occurs in the interlayer between each later, and this was added to Eqs. (2.13) for consideration.

The geometry interpolation considering the slip kinematics of n layer is obtained as

$$ {}^{t}\boldsymbol{x}^{(n)} = \sum_{k=1}^{4} h_k {}^{t}\boldsymbol{x}_k^{(n)} + \sum_{k=1}^{4}\left(m_k^{(n)} + \frac{l_k^{(n)}}{2} t^{(n)} \right) h_k {}^{t}\boldsymbol{V}_n^k + \sum_{k=1}^{4} h_k \left({}^{t}\varphi_{k,r}^{(n)t} \boldsymbol{V}_r^k + {}^{t}\varphi_{k,s}^{(n)t} \boldsymbol{V}_s^k \right) \quad , \tag{3.1} $$

with

$$ m_k^{(n)} = -\frac{a_k}{2} + \sum_{i=1}^{n} l_k^{(i)} - \frac{l_k^{(n)}}{2} \quad , $$

where h_k is the 2D shape function at node k, ${}^{t}\boldsymbol{x}_k^{(n)}$ is Cartesian coordinates of the node k in layer n, a_k is total thickness, $l_k^{(n)}$ is thickness of layer n of node k, ${}^{t}\boldsymbol{V}_n^k$ is the direction vector at node k at time t, ${}^{t}\boldsymbol{V}_r^k$ and ${}^{t}\boldsymbol{V}_s^k$ are slip direction vector at node k defined in the interlayer, ${}^{t}\varphi_{k,r}^{(n)}$ is DOF of the layer n to slip in the ${}^{t}\boldsymbol{V}_r^k$ direction, ${}^{t}\varphi_{k,s}^{(n)}$ is DOF of the layer n to slip in the ${}^{t}\boldsymbol{V}_s^k$ direction. The slip direction vector ${}^{t}\boldsymbol{V}_r^k$ is defined in the reference layer at node k.

$$ {}^{t}\boldsymbol{V}_r^k = \frac{{}^{t}\boldsymbol{g}_r^k}{\left| {}^{t}\boldsymbol{g}_r^k \right|} \quad , \tag{3.2} $$

with

$$ {}^{t}\boldsymbol{g}_r^k = \sum_{i=1}^{4} \left. \frac{\partial h(r,s)}{\partial r_1} \right|_{r=r_k} {}^{t}x_i + \sum_{i=1}^{4}\left(m_i^{(o)} + \frac{l_i^{(o)}}{2} t^{(o)} \right) \left. \frac{\partial h(r,s)}{\partial r_1} \right|_{r=r_k} {}^{t}V_n^i \quad , $$

where r_1 is natural coordinate corresponding to $r_1 = r$, the right superscript o denotes the reference layer.

The rest of the slip direction vector ${}^{t}\boldsymbol{V}_s^k$ is defined in the same way as above.

$$ {}^{t}\boldsymbol{V}_s^k = \frac{{}^{t}\boldsymbol{g}_s^k}{\left| {}^{t}\boldsymbol{g}_s^k \right|} \quad , \tag{3.3} $$

with

$$ {}^{t}g_r^k = \sum_{i=1}^{4} \frac{\partial h(r,s)}{\partial r_1}\bigg|_{r=r_k} {}^{t}x_i + \sum_{i=1}^{4} \left(m_i^{(o)} + \frac{l_i^{(o)}}{2} t^{(o)} \right) \frac{\partial h(r,s)}{\partial r_1}\bigg|_{r=r_k} {}^{t}V_n^i \quad , $$

where r_2 is natural coordinate corresponding to $r_2 = s$. A two-dimensional slip occurs in the shell element, and the slip plane is defined using two slip direction vectors.

As can be seen in Fig. 3.1, two DOF are added to each layer. First, a reference layer is randomly selected. For example, in Figure 3.1, layer 1 is the reference layer. First, the degree of freedom ${}^{t}\varphi_{r,k}^{(n)}$ at node k is the discontinuity of displacement between the reference layer and the layer n in the slip direction vector ${}^{t}V_r^k$. Similarly, the displacement discontinuity of the reference layer and layer n in the ${}^{t}V_s^k$ direction becomes the ${}^{t}\varphi_{s,k}^{(n)}$ (See Fig. 3.2).

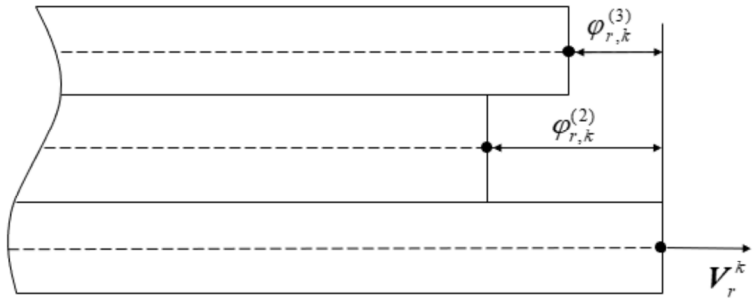

(a)

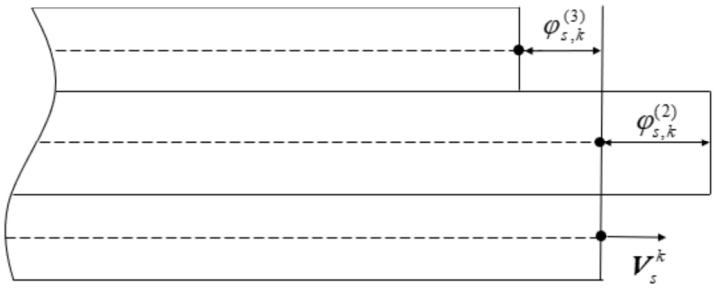

(b)

Fig. 3.2. Definition of slip direction vector and layer DOF

From the added degree of freedom, the slip displacement interpolations in interlayer i are obtained as:

$$ {}^{t}u_{r}^{(i)} = \sum_{k=1}^{4} h_k \left({}^{t}\varphi_{k,r}^{(n_2)} - {}^{t}\varphi_{k,r}^{(n_1)} \right) \quad , \tag{3.4} $$

$$ {}^{t}u_{s}^{(i)} = \sum_{k=1}^{4} h_k \left({}^{t}\varphi_{k,s}^{(n_2)} - {}^{t}\varphi_{k,s}^{(n_1)} \right) \quad , \tag{3.5} $$

where i is interlayer between layers n_1 and n_2.

The displacement interpolation of 4-node shell element in layer n from the configuration at a given time t and original configuration. is obtained by

$$ \begin{aligned} {}^{t}\boldsymbol{u}^{(n)} = & \sum_{k=1}^{4} h_k {}^{t}u_k^{(n)} + \sum_{k=1}^{4} \left(m_k^{(n)} + \frac{l_k^{(n)}}{2} t^{(n)} \right) h_k (-\alpha_k {}^{0}\boldsymbol{V}_2^k + \beta_k {}^{0}\boldsymbol{V}_1^k) \\ & + \sum_{k=1}^{4} h_k \left({}^{t}\varphi_{k,r}^{(n)t}\boldsymbol{V}_r^k - {}^{0}\varphi_{k,r}^{(n)0}\boldsymbol{V}_r^k + {}^{t}\varphi_{k,s}^{(n)t}\boldsymbol{V}_s^k - {}^{0}\varphi_{k,s}^{(n)0}\boldsymbol{V}_s^k \right), \end{aligned} \tag{3.6} $$

where $u_k^{(n)}$ is incremental node displacement from original configuration to current configuration at given time t.

Using the slip direction vector in the original configuration, the final slip direction vector is approximated as:

$$ \begin{aligned} {}^{t}\boldsymbol{V}_r^k &= \frac{{}^{t}\boldsymbol{g}_r^k}{\left| {}^{t}\boldsymbol{g}_r^k \right|} \\ &\simeq {}^{0}\boldsymbol{V}_r^k + \frac{1}{\left| {}^{0}\boldsymbol{g}_r^k \right|} \left\{ \sum_{i=1}^{4} \left. \frac{\partial h_i}{\partial r_1} \right|_{r=r_k} u_i + \sum_{i=1}^{4} \left. \frac{\partial h_i}{\partial r_1} \right|_{r=r_k} (m_i^{(o)} + \frac{l_i^{(o)}}{2} t^{(o)})(-\alpha_i {}^{0}V_2^i + \beta_i {}^{0}V_1^i) \right\} \end{aligned} \tag{3.7} $$

and

$$ \begin{aligned} {}^{t}\boldsymbol{V}_s^k &= \frac{{}^{t}\boldsymbol{g}_s^k}{\left| {}^{t}\boldsymbol{g}_s^k \right|} \\ &\simeq {}^{0}\boldsymbol{V}_s^k + \frac{1}{\left| {}^{0}\boldsymbol{g}_s^k \right|} \left\{ \sum_{i=1}^{4} \left. \frac{\partial h_i}{\partial r_2} \right|_{r=r_k} u_i + \sum_{i=1}^{4} \left. \frac{\partial h_i}{\partial r_2} \right|_{r=r_k} (m_i^{(o)} + \frac{l_i^{(o)}}{2} t^{(o)})(-\alpha_i {}^{0}V_2^i + \beta_i {}^{0}V_1^i) \right\}. \end{aligned} \tag{3.8} $$

where ${}^0\boldsymbol{g}_r^k$ and ${}^0\boldsymbol{g}_s^k$ are covariant base vector in the original configuration, r_1 and r_2 are natural coordinate corresponding to $r_1 = r$, $r_2 = s$.

Substituting Eqs. (3.7) and (3.8) into Eqs. (3.6), the displacement interpolation is derived as

$$
\begin{aligned}
{}^t\boldsymbol{u}^{(n)} = & \sum_{k=1}^{4} h_k {}^t u_k^{(n)} + \sum_{k=1}^{4}\left(m_k^{(n)} + \frac{l_k^{(n)}}{2} t^{(n)} \right) h_k (-\alpha_k {}^0\boldsymbol{V}_2^k + \beta_k {}^0\boldsymbol{V}_1^k) \\
& + \sum_{k=1}^{4} h_k \left({}_0\varphi_{k,r}^{(n)0}\boldsymbol{V}_r^k + ({}_0\varphi_{k,r}^{(n)} + {}_0^t\varphi_{k,r}^{(n)}) \frac{1}{\left| {}^0 g_r^k \right|} \sum_{i=1}^{4} \left. \frac{\partial h_i}{\partial r_1} \right|_{r=r_k} (u_i + (m_i^{(o)} + \frac{l_i^{(o)}}{2} t^{(o)})(-\alpha_i {}^0V_2^i + \beta_i {}^0V_1^i)) \right) \\
& + \sum_{k=1}^{4} h_k \left({}_0\varphi_{k,s}^{(n)0}\boldsymbol{V}_s^k + ({}_0\varphi_{k,s}^{(n)} + {}_0^t\varphi_{k,s}^{(n)}) \frac{1}{\left| {}^0 g_s^k \right|} \sum_{i=1}^{4} \left. \frac{\partial h_i}{\partial r_2} \right|_{r=r_k} (u_i + (m_i^{(o)} + \frac{l_i^{(o)}}{2} t^{(o)})(-\alpha_i {}^0V_2^i + \beta_i {}^0V_1^i)) \right)
\end{aligned}
\tag{3.9}
$$

where ${}_0\varphi_{k,r}^{(n)}$ and ${}_0\varphi_{k,s}^{(n)}$ are the incremental DOF to the layer n. After linearization, equation 3.9 applying first-order approximation, incremental displacement of layer n is obtained as

$$
\begin{aligned}
{}^t\boldsymbol{u}^{(n)} = & \sum_{k=1}^{4} h_k {}^t u_k^{(n)} + \sum_{k=1}^{4}\left(m_k^{(n)} + \frac{l_k^{(n)}}{2} t^{(n)} \right) h_k (-\alpha_k {}^0\boldsymbol{V}_2^k + \beta_k {}^0\boldsymbol{V}_1^k) \\
& + \sum_{k=1}^{4} h_k \left({}_0\varphi_{k,r}^{(n)0}\boldsymbol{V}_r^k + \frac{{}_0^t\varphi_{k,r}^{(n)}}{\left| {}^0 g_r^k \right|} \sum_{i=1}^{4} \left. \frac{\partial h_i}{\partial r_1} \right|_{r=r_k} (u_i + (m_i^{(o)} + \frac{l_i^{(o)}}{2} t^{(o)})(-\alpha_i {}^0V_2^i + \beta_i {}^0V_1^i)) \right) \\
& + \sum_{k=1}^{4} h_k \left({}_0\varphi_{k,s}^{(n)0}\boldsymbol{V}_s^k + \frac{{}_0^t\varphi_{k,s}^{(n)}}{\left| {}^0 g_s^k \right|} \sum_{i=1}^{4} \left. \frac{\partial h_i}{\partial r_2} \right|_{r=r_k} (u_i + (m_i^{(o)} + \frac{l_i^{(o)}}{2} t^{(o)})(-\alpha_i {}^0V_2^i + \beta_i {}^0V_1^i)) \right).
\end{aligned}
\tag{3.10}
$$

3.2. **The principle of virtual work**

For finite element analysis, the principle of virtual work is introduced briefly. The concept of virtual work is that external virtual work done by surface traction and body force is equal to internal virtual work done by the internal force as shown by

$$\int_V \tau_{ij}\delta\varepsilon_{ij}dV = \int_V f_i^B \delta u_i dV + \int_S f_i^S \delta u_i dS \quad , \tag{3.11}$$

where δu denotes virtual displacement, $\delta\varepsilon$ is virtual strains, f^B and f^S are the body force and surface traction, respectively

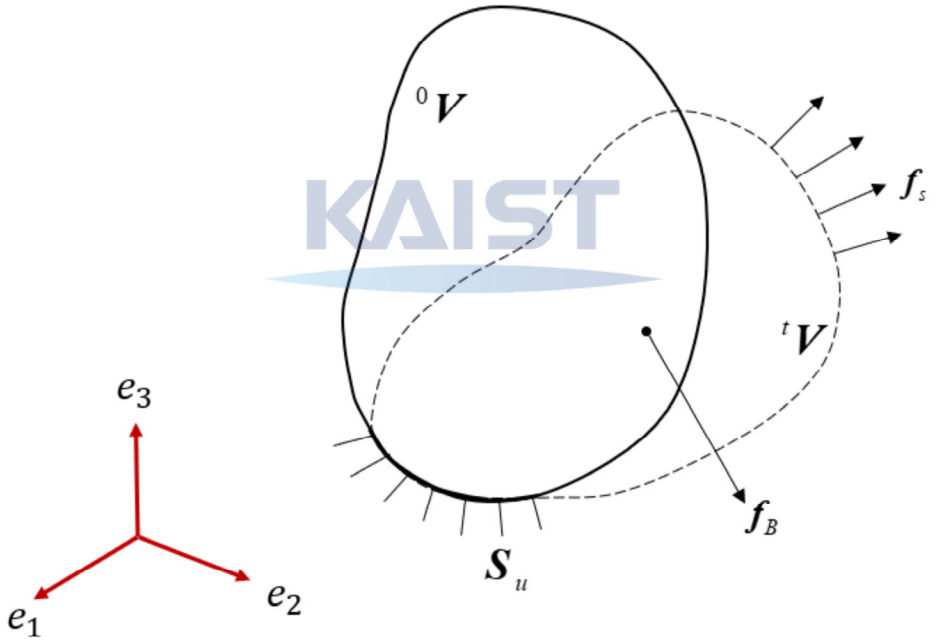

Fig. 3.3. Geometry of 4-node shell element with interlayer slip

In the interlayer, the partial interaction is modeled with a constant slip modulus K_s, and considering only the linear component in the Green Lagrange strain, it is as follows:

$$\boldsymbol{F}_s = \boldsymbol{K}_{slip}\boldsymbol{u}_{slip} \quad , \tag{3.12}$$

and

$$\boldsymbol{\tau} = \boldsymbol{C}\boldsymbol{\varepsilon} \quad . \tag{3.13}$$

where $\boldsymbol{F}_s$ is slip force defined in the interlayer, u_{slip} is slip displacement, $\boldsymbol{C}$ is the stress-strain matrix of material property. Substituting the Eqs. (3.11) into Eqs. (3.10), the week form of the principle of virtual work is expressed as

$$\int_V \delta\boldsymbol{\varepsilon}^T \boldsymbol{C}\boldsymbol{\varepsilon} dV + \int_A \delta\boldsymbol{u}_{slip}{}^T \boldsymbol{K}_{slip}\boldsymbol{u}_{slip} dA = \int_V \delta\boldsymbol{u}^T \boldsymbol{f}^B dV + \int_S \delta\boldsymbol{u}^T \boldsymbol{f}^S dS \quad , \tag{3.14}$$

with

$$u_{slip} = \begin{pmatrix} u_r & \cdots \\ \cdots & u_s \end{pmatrix} \quad ,$$

$$\boldsymbol{K}_{slip} = \begin{bmatrix} K_s & 0 \\ 0 & K_s \end{bmatrix} \quad .$$

where u_r is slip displacement in the $\boldsymbol{V}_r$ direction, u_s is slip displacement in the $\boldsymbol{V}_s$ direction, K_s is slip modulus.

The final formulation by implementing the layered model is as follows

$$\begin{aligned} &\sum_n \int_{V^{(n)}} \overline{\boldsymbol{C}}_{ijkl}^{(n)} \overline{\boldsymbol{e}}_{ij}^{(n)} \delta\overline{\boldsymbol{e}}_{kl}^{(n)} dV + \sum_i \int_A \boldsymbol{K}_{slip}^{(i)} \boldsymbol{u}_{slip}^{(i)} \delta\boldsymbol{u}_{slip}^{(i)} dA \\ &\qquad = \sum_n \int_V \delta\boldsymbol{u}^{(n)T} \boldsymbol{f}^{(n)^B} dV + \sum_n \int_S \delta\boldsymbol{u}^{(n)T} \boldsymbol{f}^{(n)^S} dS. \end{aligned} \tag{3.15}$$

3.3. **Finite element analysis of layered shell formulation**

In Chapter 2.2, the linear parts of the Green-Lagrange strain in the configuration from original time 0 to given time t is given by

$$ {}^{t}_{0}\tilde{e}^{(n)}_{ij} = \frac{1}{2}({}^{t}\boldsymbol{g}^{(n)}_{i}\frac{\partial_0 \boldsymbol{u}^{(n)}}{\partial r_j} + {}^{t}\boldsymbol{g}^{(n)}_{j}\frac{\partial_0 \boldsymbol{u}^{(n)}}{\partial r_i}) \quad , \tag{3.16} $$

$$ {}^{t}_{0}\bar{e}^{(n)}_{ij} = (\hat{\boldsymbol{e}}_i \cdot {}^{0}\boldsymbol{g}^{k(n)})(\hat{\boldsymbol{e}}_j \cdot {}^{0}\boldsymbol{g}^{l(n)})\,{}_{0}\tilde{e}^{(n)}_{kl} \quad , \tag{3.17} $$

with

$$ {}^{t}\boldsymbol{g}^{(n)}_{i} = \frac{\partial {}^{t}\boldsymbol{x}^{(n)}}{\partial r_i} \quad . $$

where r_i is natural coordinate corresponding to $r_1 = r$, $r_2 = s$, $r_3 = t^{(n)}$.

The strain-displacement matrix B in the local Cartesian coordinate system is obtained as

$$ {}^{t}_{0}\bar{e}^{(n)}_{ij} = \overline{\boldsymbol{B}}^{(n)}_{ij}\boldsymbol{U} \quad , \tag{3.18} $$

with

$$ \boldsymbol{U} = [u_1 \ \cdots \ v_1 \ \cdots \ w_1 \ \cdots \ \alpha_1 \ \cdots \ \beta_1 \ \cdots \ \varphi^{(1)}_{r,1} \ \cdots \ \varphi^{(1)}_{s,1} \ \cdots \ \varphi^{(n)}_{r,1} \ \cdots \ \varphi^{(n)}_{r,4} \ , \ \varphi^{(n)}_{s,1} \ \cdots \ \varphi^{(n)}_{s,4}]^T $$

Unlike Eqs. (2.17), it can be seen that the degree of freedom of each layer has been added. Here, the degree of freedom of the randomly selected reference layer is 0.

Likewise, the slip displacement defined in the interlayer is interpolated

$$ {}^{t}u^{(i)}_{r} = \sum_{k=1}^{4} h_k(r,s)\left({}^{t}\varphi^{(n_2)}_{k,r} - {}^{t}\varphi^{(n_1)}_{k,r}\right) = \boldsymbol{H}^{(i)}_{s,1}\boldsymbol{U} \quad , \tag{3.19} $$

$$ {}^{t}u^{(i)}_{s} = \sum_{k=1}^{4} h_k(r,s)\left({}^{t}\varphi^{(n_2)}_{k,s} - {}^{t}\varphi^{(n_1)}_{k,s}\right) = \boldsymbol{H}^{(i)}_{s,2}\boldsymbol{U} \quad , \tag{3.20} $$

$$ \boldsymbol{H}^{(i)}_{s} = \begin{pmatrix} \boldsymbol{H}^{(i)}_{s,1} \\ \boldsymbol{H}^{(i)}_{s,2} \end{pmatrix} \quad , \tag{3.21} $$

where $\boldsymbol{H}_s^{(i)}$ is the slip displacement matrix at interlayer i, n_1 and n_2 denote adjacent layer that make up the interlayer i.

The virtual Green-Lagrange strains and interlayer slip displacement are summarized

$$\delta_0^t \overline{e}_{ij}^{(n)} = \overline{\boldsymbol{B}}_{ij}^{(n)} \delta \boldsymbol{U} \,, \tag{3.22}$$

$$\delta \boldsymbol{u}_s^{(i)} = \boldsymbol{H}_s^{(i)} \delta \boldsymbol{U}. \tag{3.23}$$

By substituting the Eqs. (3.18)~(3.23) into Eqs. (3.15), The formulation of finite element is obtained as

$$\boldsymbol{K}\boldsymbol{U} = \boldsymbol{R}\,, \quad \boldsymbol{K} = \boldsymbol{K}_L + \boldsymbol{K}_S \tag{3.24}$$

where

$$\boldsymbol{K}_L = \sum_n \int_{V^{(n)}} \overline{B}_{ij}^{(n)^T} \overline{C}_{ijkl}^{(n)} \overline{B}_{kl}^{(n)} dV^{(n)} \quad , \tag{3.25}$$

$$\boldsymbol{K}_S = \sum_i \int_{A^{(i)}} \boldsymbol{H}_s^{(i)^T} \boldsymbol{K}_s^{(i)} \boldsymbol{H}_s^{(i)} dA \quad , \tag{3.26}$$

$$\boldsymbol{R} = \sum_n \int_V \boldsymbol{H}^{(n)} \boldsymbol{f}^{(n)^B} dV + \sum_n \int_S \boldsymbol{H}^{(n)} \boldsymbol{f}^{(n)^S} dS \,. \tag{3.27}$$

Chapter 4. Numerical Example

In this chapter, various numerical examples are examined to confirm the performance of the proposed shell element considering interlayer slip. For accurate verification the most important numerical results of the presented model, such as displacement at the end of the model, are compared with a reference. As a reference, a solid element of ADINA, a commercial tool considering the physical properties of the adhesive interlayer such as connection stiffness, is used.

4.1. Two-layers cantilever

Tip displacement according to the partial interaction between layers in a two-layer composite cantilever are compared. First the connection stiffness was set to 0, the numerical example, which is a complete slip condition, are confirmed. Next, when the connection stiffness is very large, the behavior is compared under rigid interlayer conditions. Finally, when the connection stiffness has an arbitrary value, the behavior under axial load and vertical load are compared respectively with the reference model.

4.1.1. Perfectly slip with no connection stiffness

In Fig. 4.1 and Fig. 4.2, it can be seen that the y-axis load was applied to layer 2 in a two-layer composite shell without connection stiffness.

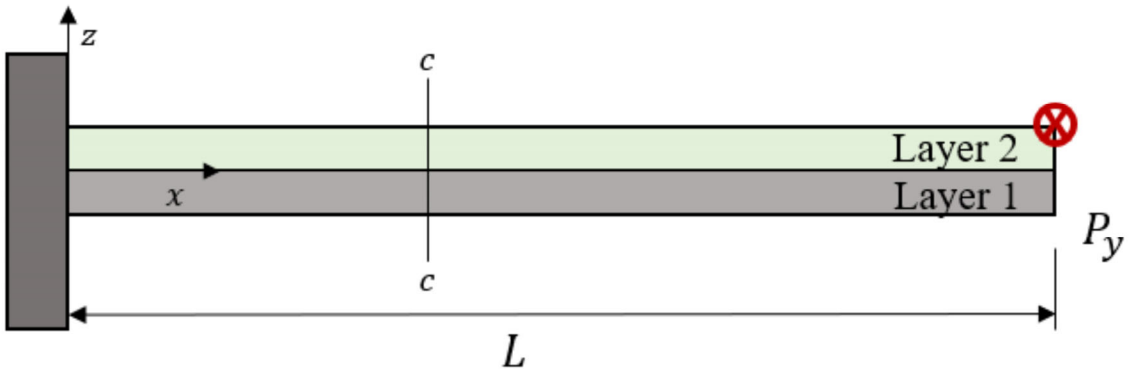

(a)

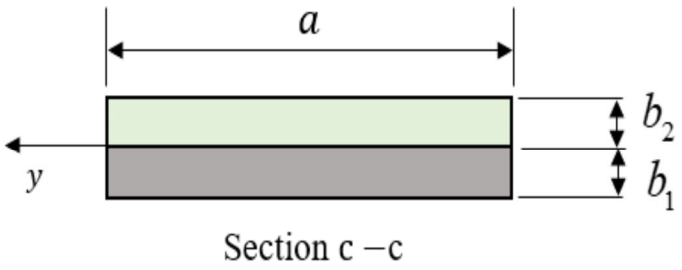

(b)

Fig. 4.1. Geometry of two-layer cantilever: (a) Problem description (b) Cross section c-c

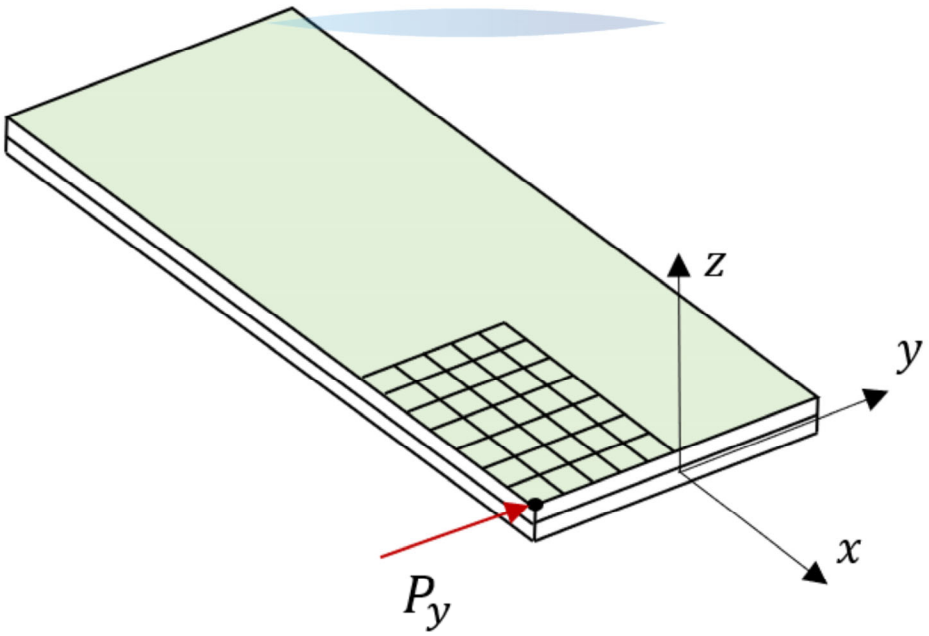

Fig. 4.2. Loading condition with perfectly slip

Each shell has the same material properties and geometry values. Table 4.1 shows geometry, loading condition and material properties.

Table 4.1. Material property, geometry condition, loading condition of Fig. 4.1 and Fig. 4.2

Material property
$E_1 = 200$ GPa, $E_2 = 200$ GPa, $v_1 = v_2 = 0.3$, $K_s = 0$ N/m^2
Geometry condition
$L = 2\,m$, a $= 1\,m$, $b_1 = b_2 = 0.02$ m
Loading condition
$P_y = 500$N

Since there is no connection stiffness, the two-layer behaviors are different when y-axis load is applied. Fig. 4.3 shows the result of comparing the behavior of the shell element corresponding to one layer as a reference. Layer 1 do not behave at all, and layer 2 shows the same result as the reference.

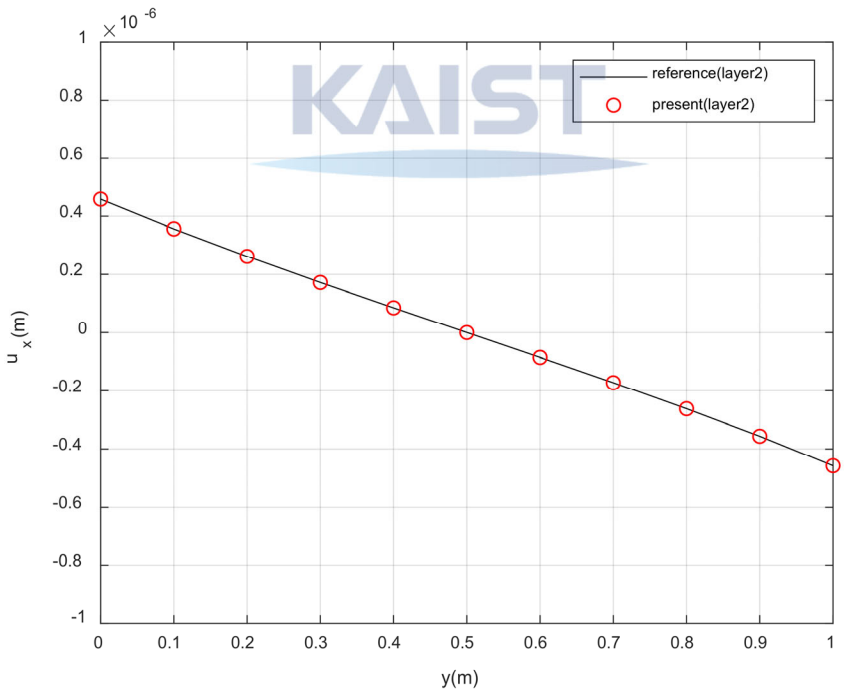

(a)

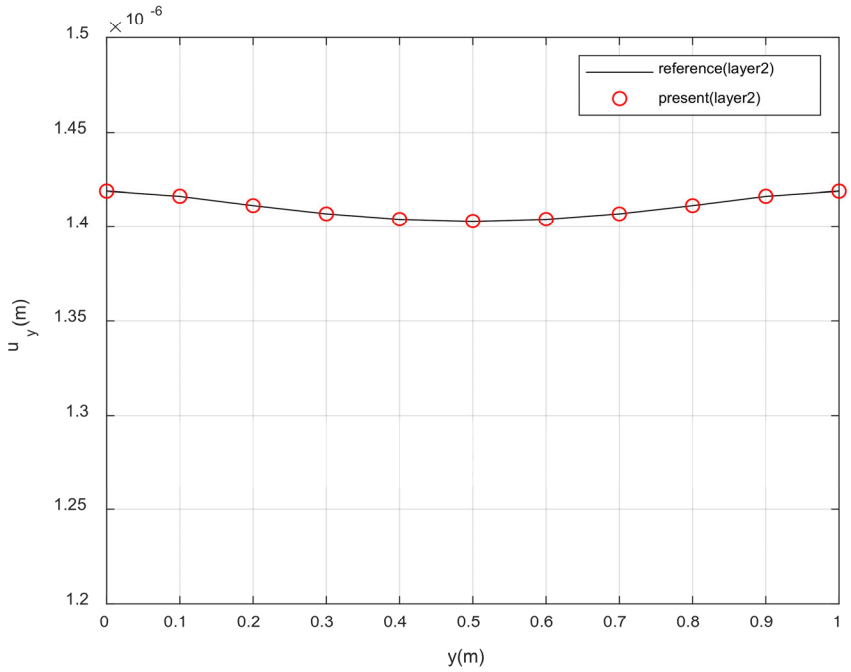

(b)

Fig. 4.3. Displacement at the tip: (a) Displacement of x (b) Displacement of y

4.1.2. No interlayers with perfect connection

The two layers are completely combined, so the shell model without interlayer is shown in Fig. 4.4.

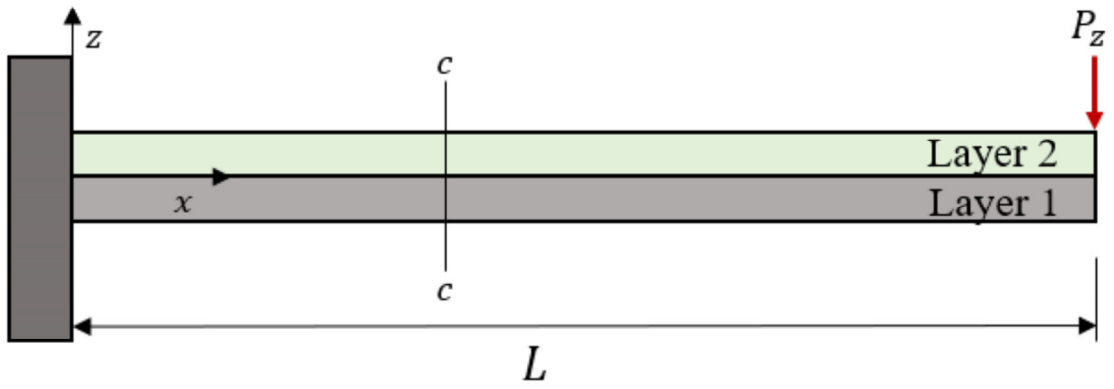

(a)

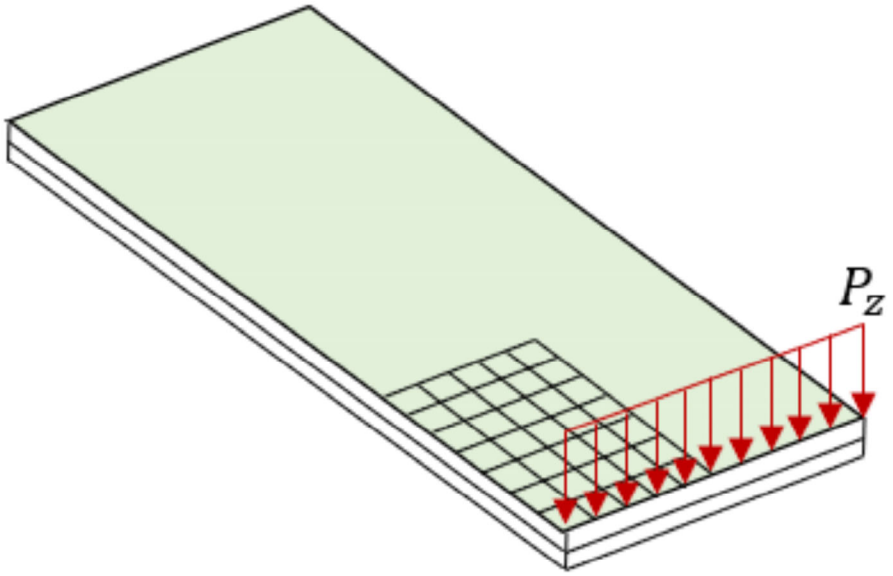

(b)

Fig. 4.4. Problem description: (a) Geometry condition (b) Loading condition

Unlike the example in 4.1.1, a vertical load is applied to a composite model with different properties of each layer. Table 4.2 summarizes the material property, geometry and loading condition. It can be seen that the connection stiffness is very large to express that the layers are completely combined.

Table 4.2. Material property, geometry condition, loading condition of Fig. 4.4

Material property
$E_1 = 200$ GPa, $E_2 = 50$ GPa, $v_1 = v_2 = 0.3$, $K_s = 5 \times 10^{20}$ N/m^2
Geometry condition
$L = 2\,m$, a $= 1\,m$, $b_1 = b_2 = 0.02$ m
Loading condition
$P_z = 500$N

The deflection at the tip of the cantilever at this loading condition is shown in Fig. 4.5. As a reference, a composite shell element in ADINA that don't implement slip was used. When comparing the deflection according to y at the end, the proposed element agrees well with the reference result.

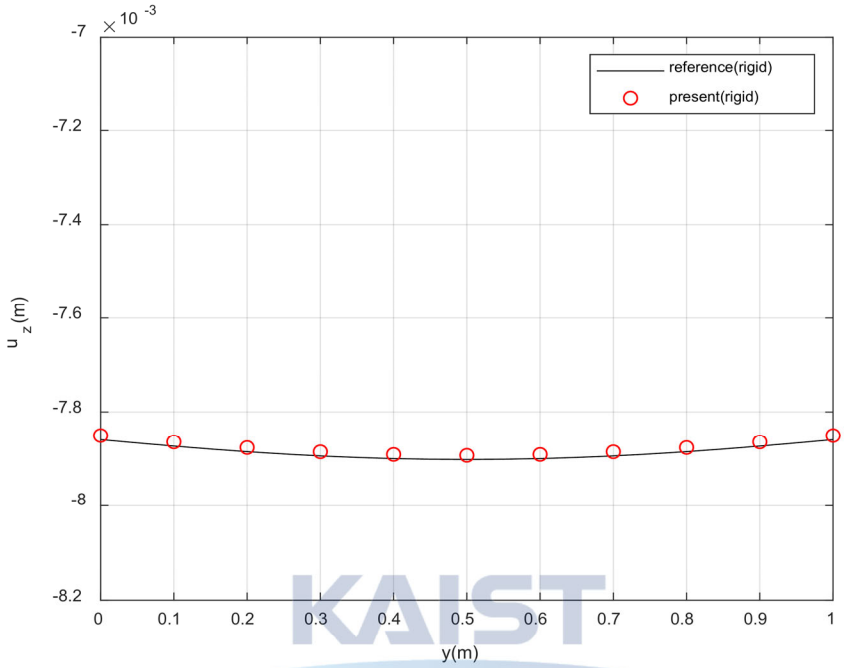

Fig. 4.5. deflection at the tip of cantilever

4.1.3. Two-layer cantilever behavior with constant connection stiffness.

The last thing to be seen in the two-layer cantilever example is its behavior when axial and vertical loads are applied. In Fig. 4.6.(a), the axial load is applied, and in Fig. 4.6.(b), the vertical load is applied.

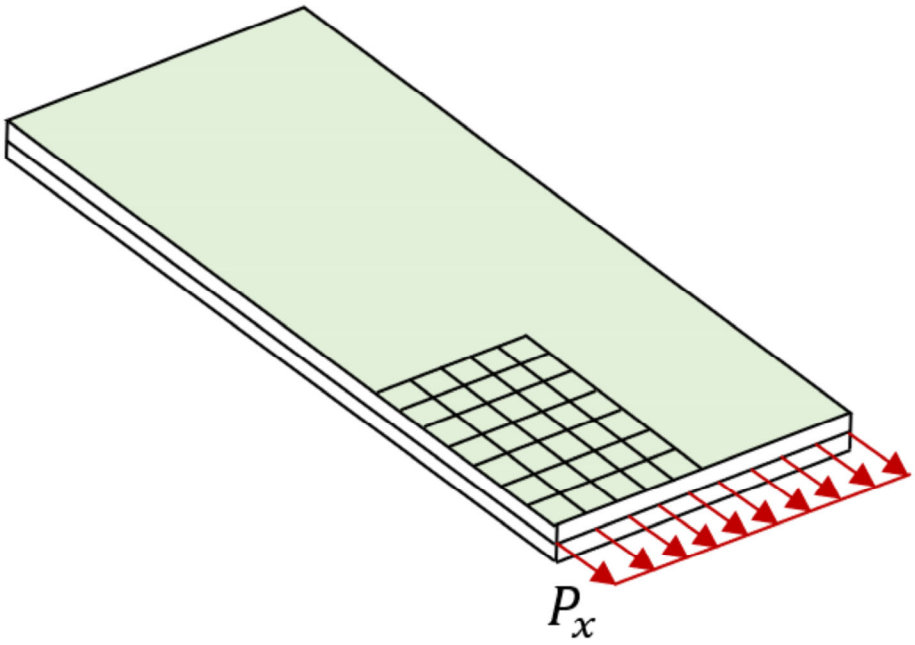

(a)

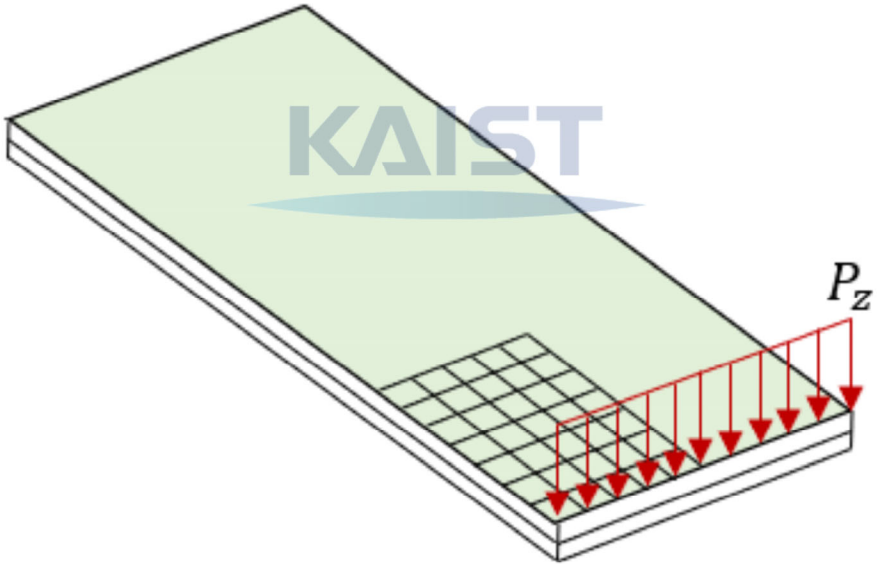

(b)

Fig. 4.6. Loading condition with constant connection stiffness: (a) Axial loading condition (b) Vertical loading condition

In both loading conditions, the geometry conditions are the same. The geometry, loading conditions and material properties are identified in Table 4.3. The connection stiffness was set to a random value other than 0.

Table 4.3. Material property, geometry condition, loading condition of Fig. 4.6

Material property
$E_1 = 200$ GPa, $E_2 = 50$ GPa, $v_1 = v_2 = 0.3$, $K_s = 10$ MN/m^2
Geometry condition
$L = 2\,m$, a $= 1\,m$, $b_1 = b_2 = 0.02$ m
Loading condition
$P_x = 500\,N$ $P_z = 500$ N

A two-layer cantilever is modeled using 200 shell elements. For the reference, ADINA solid elements with cohesive material are used. In Fig. 4.6.(a), modeling is performed using 20,000 elements. The reference in Fig. 4.6.(b) uses 1,500,000 elements. Figure 4.7 (a) and (b) show the result of comparing the x and y displacements at the ends under axial load. Figure 4.8 shows the result of comparing the deflection of the reference and the proposed element under vertical load. All three results show good agreement between proposed element and the reference model.

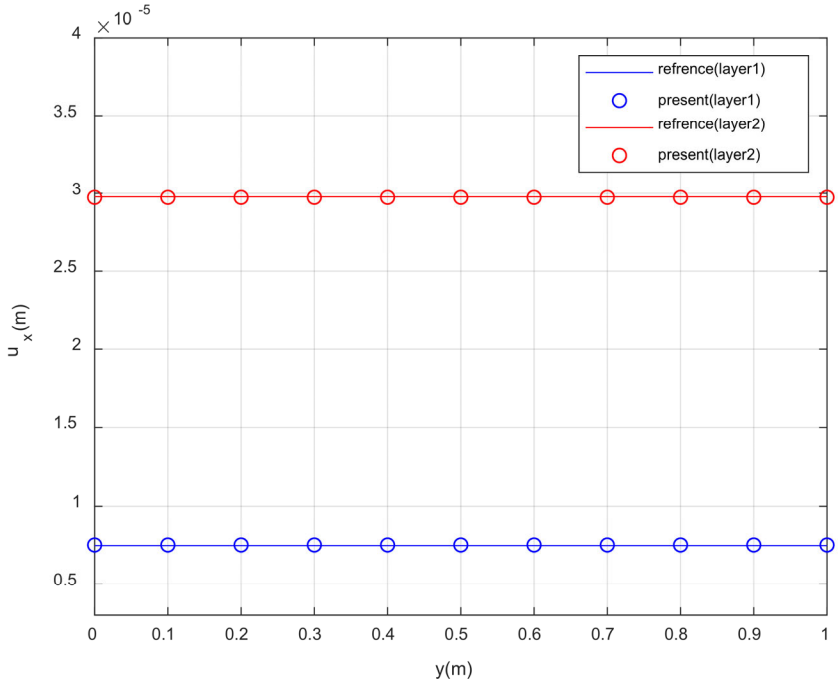

(a)

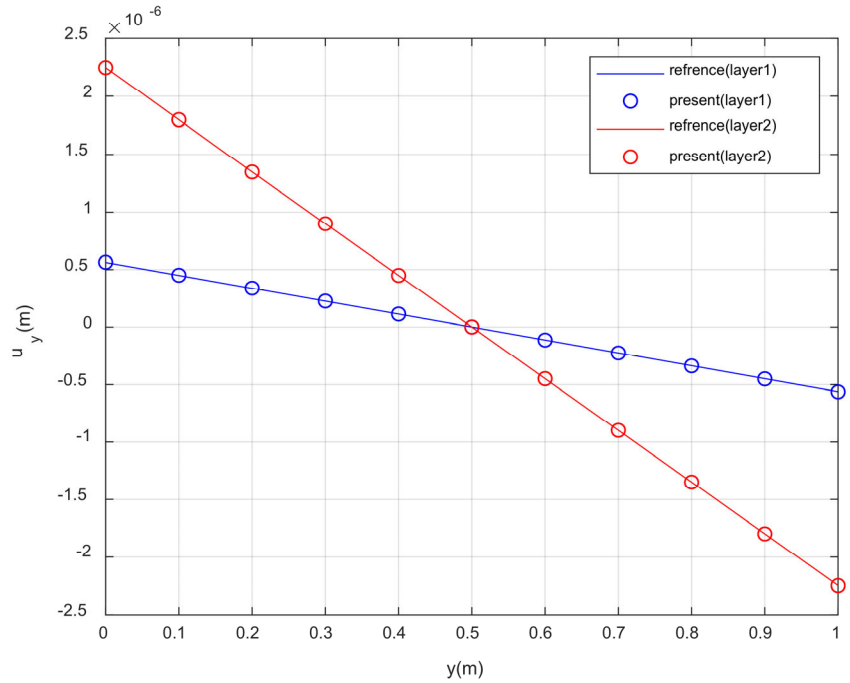

(b)

Fig. 4.7. Displacement at the tip with axial load: (a) Displacement of x (b) Displacement of y

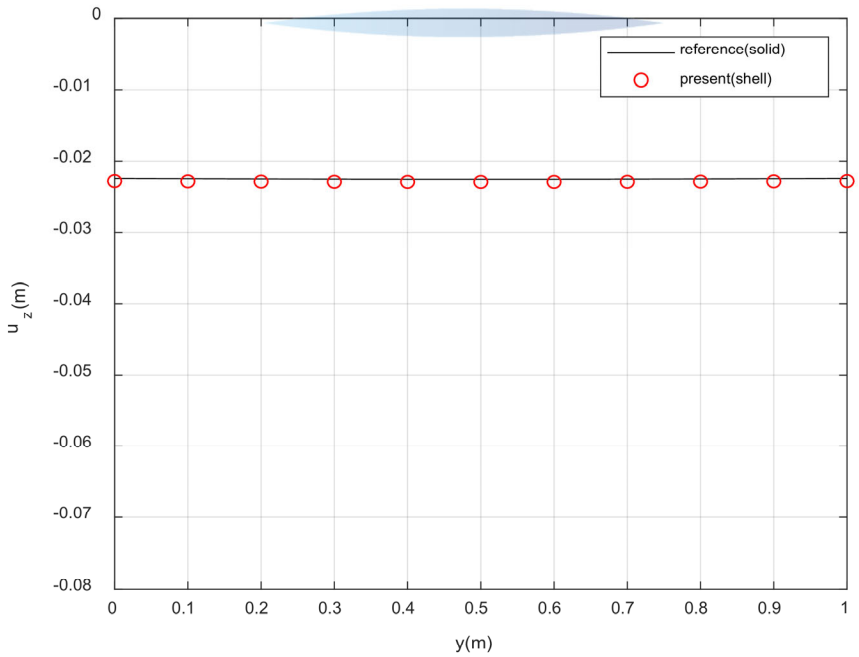

Fig. 4.8. Deflection at the tip with vertical load

4.2. **Three-layers cantilever**

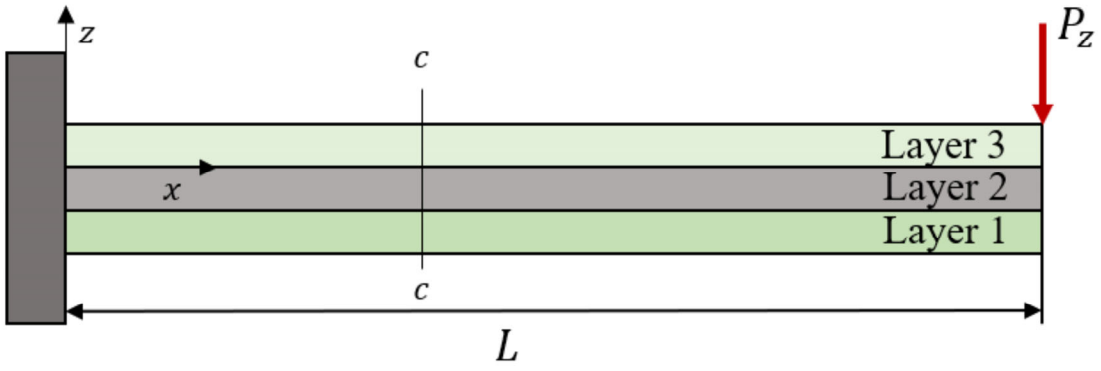

(a)

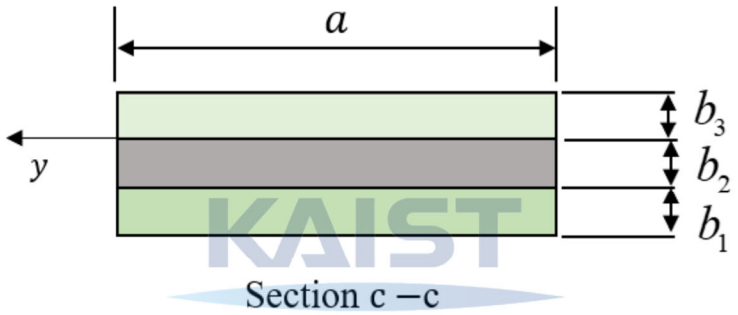

(b)

Fig. 4.9. Geometry condition of three layers cantilever: (a) Problem description (b) Cross section c-c

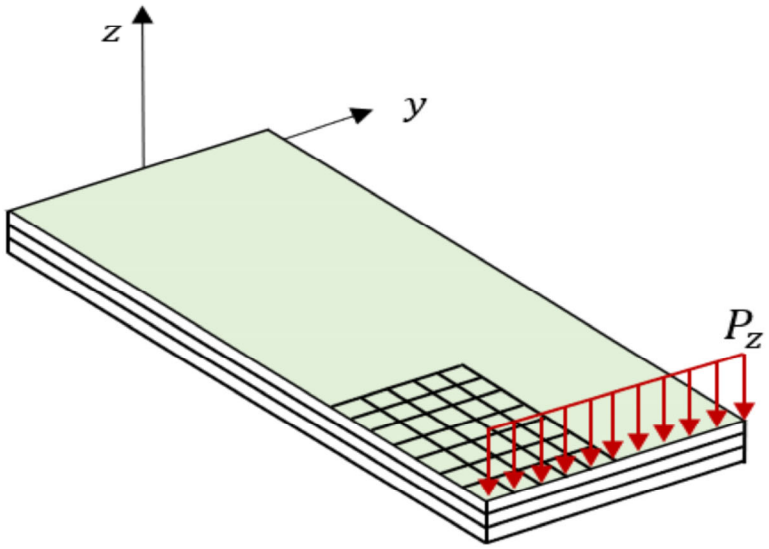

Fig. 4.10. Vertical loading condition of Fig. 4.9.

A three-layers cantilever example is reviewed to see if the proposed element can be used for multiple-layers as well. In this example, three shell elements are stacked and different connection stiffnesses are considered for each interlayer. Fig. 4.9 shows the geometry of the three-layer cantilever, and Fig. 4.10 shows detailed loading conditions. The numerical values for material properties, geometry and loading conditions are shown in Table 4.4.

Table 4.4. Material property, geometry condition, loading condition of Fig. 4.9 and Fig. 4.10.

Material property
$E_1 = 10$ GPa, $E_2 = 50$ GPa, $E_3 = 200$ GPa, $v_1 = v_2 = v_3 = 0.3$, $K_s^1 = 1 \times 10^8$ N/m^2, $K_s^2 = 2 \times 10^8$ N/m^2
Geometry condition
$L = 2\,m$, a $= 1\,m$, $b_1 = b_2 = b_3 = 0.02$ m
Loading condition
$P_z = 1500$ N

To model the three-layer laminated shell, 200 proposed elements are used. Each additional layer adds 8 DOF per element. As a reference, it was modeled using ADINA solid elements that considered cohesive properties. In order to model a thin cantilever as a solid, accurate results could be achieved only when many elements are used in the thickness direction. Thus about 2,000,000 solid elements are used to construct this example. Figure 4.11 compares the deflection of the reference and the proposed element at the end of the cantilever. Comparing the deflection along the y-axis at the ends, the new layered shell element exhibited good agreement with the reference.

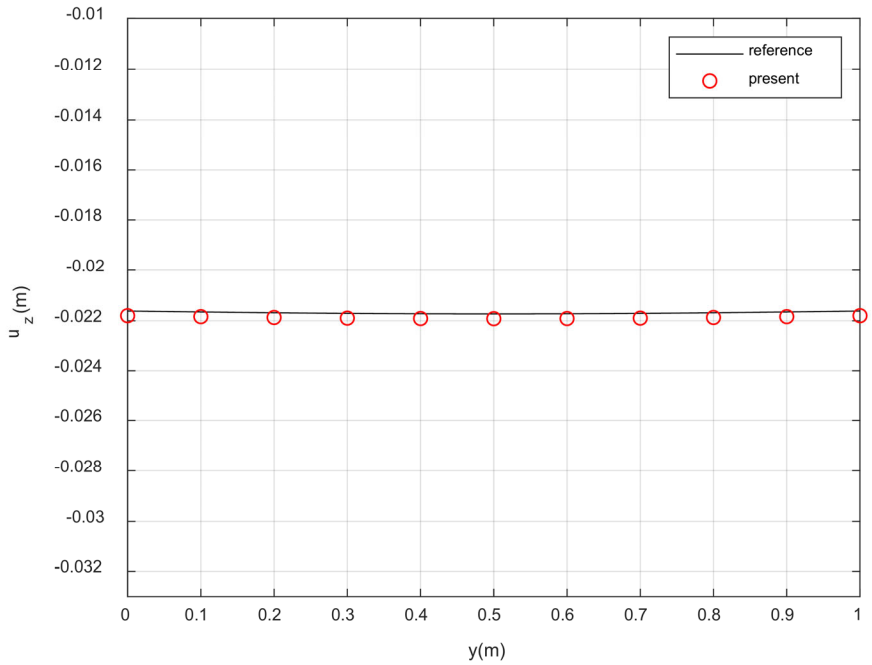

Fig. 4.11. deflection at the tip in three-layered composite shell

4.3. **Quarter cylinder**

Departing from the simple cantilever, a vertical load is applied to the quarter cylinder to check the curvature example. Fig 4.12. shows the z-direction load applied to the end of the quarter cylinder with radius R. In addition, detailed numerical values for material properties, geometry and loading condition are displayed in Table 4.5.

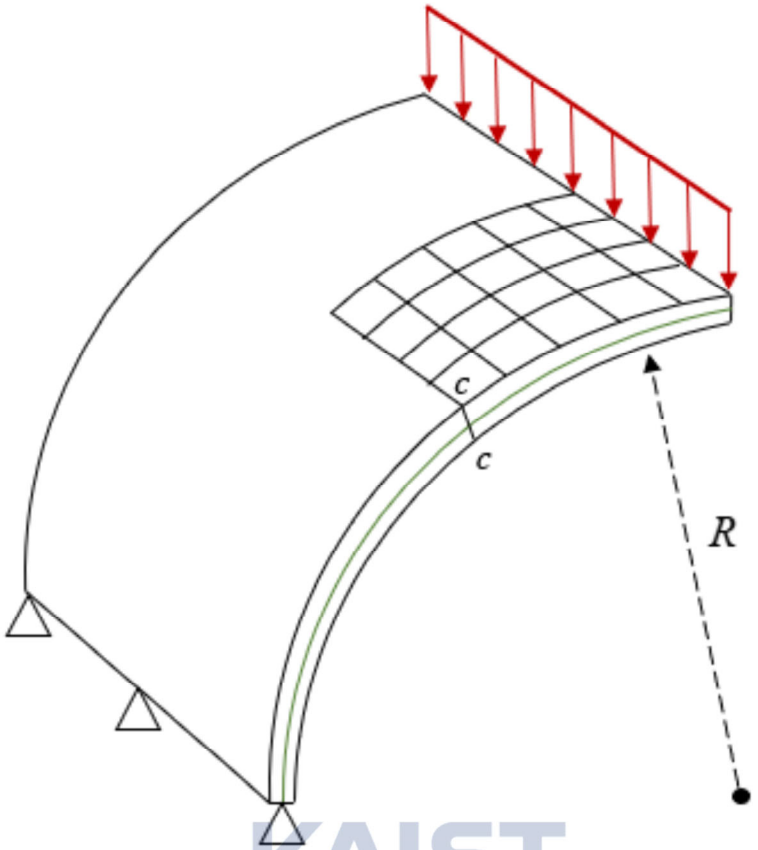

(a)

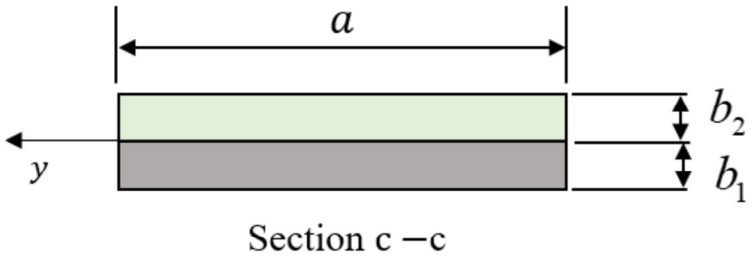

(b)

Fig. 4.12. Geometry and loading condition of quarter cylinder: (a) Problem description (b) Cross section c-c

Table 4.5. Material property, geometry condition, loading condition of Fig. 4.12.

Material property
$E_1 = 200$ GPa, $E_2 = 50$ GPa, $v_1 = v_2 = 0.3$, $K_s = 10$ MN/m^2
Geometry condition
R $= 1\,m$, a $= 1\,m$, $b_1 = b_2 = 0.03$ m
Loading condition
$P_z = 500$ N

Like the previous example, a cylinder is constructed using 200 proposed shell elements. For the reference, 800,000 ADINA solid element are used that were considered cohesive. Figure 4.13 shows the result of comparing the z-direction displacement at the end of the cylinder. When compared with the reference solution, good agreement with the proposed element was observed.

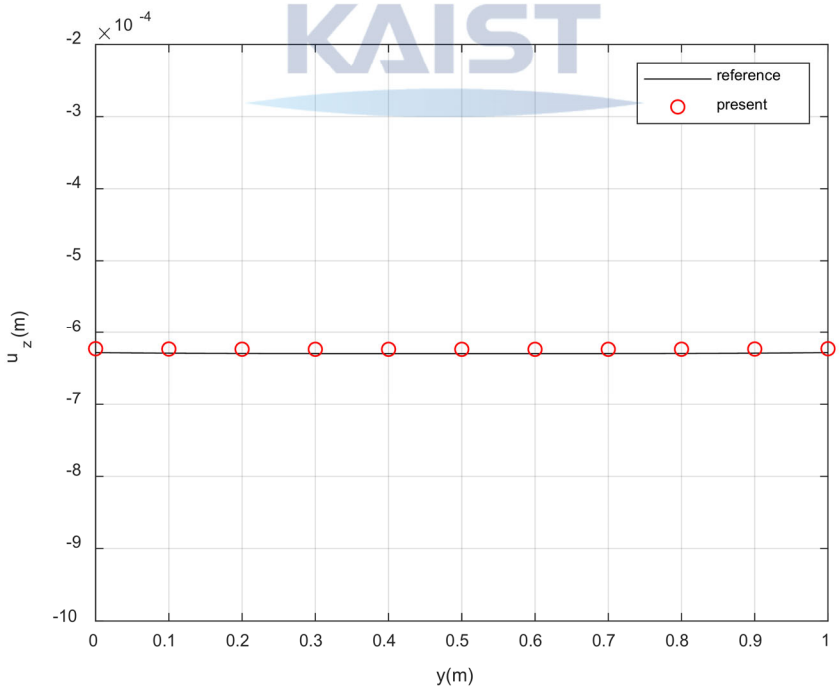

Fig. 4.13. Displacement of z-direction at the end line

4.4. **Shallow composite panel**

The examples so far show that the displacement is almost unchanged along the y-axis. In order to confirm the two-Dimensional slip, the thin composite panel analysis is performed. Figure 4.14 shows a concentrated load applied in the middle of a shallow composite panel. Further details such as material properties, geometry and loading conditions can be found in Table 4.6.

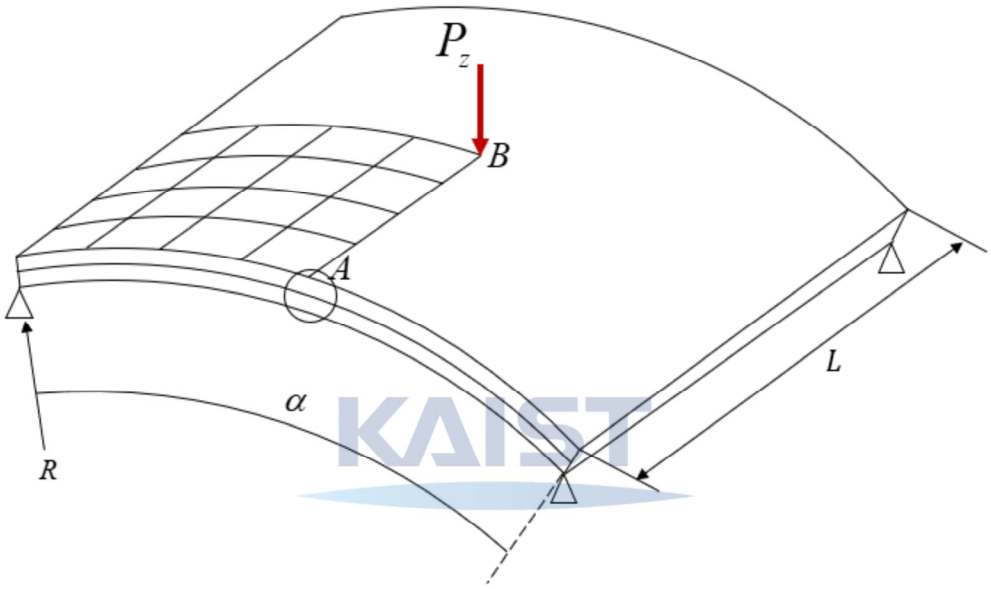

(a)

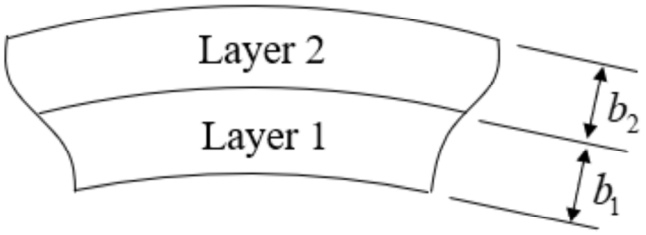

(b)

Fig. 4.14. Geometry and loading condition of shallow panel: (a) Problem description (b) thickness of composite model

Table 4.6. Material property, geometry condition, loading condition of Fig. 4.14.

Material property
$E_1 = 0.5\ GPa,\ E_2 = 1\ \text{GPa},\ v_1 = v_2 = 0.3,\ K_s = 1\ \text{MN/m}^2$
Geometry condition
$L = 0.5\ m,\ R = 2.5\ m,\ \alpha = 0.02\ \text{rad},\ b_1 = b_2 = 0.04\ \text{m}$
Loading condition
$P_z = 500\ \text{N}$

Structure analysis of two-layer shallow composite panel was conducted using 100 proposed shell elements. Using 70000 solid elements in ADINA, the amount of deflection at the center line when applied to a load in the middle of a thin panel was checked and used as a reference. Fig. 4.15 shows the comparison of the deflection curve of the line AB of the reference and the proposed element. The red circle is the suggested element, and the black straight line is the reference using the solid element. It is confirmed that it agrees well with the parabolic result of the reference.

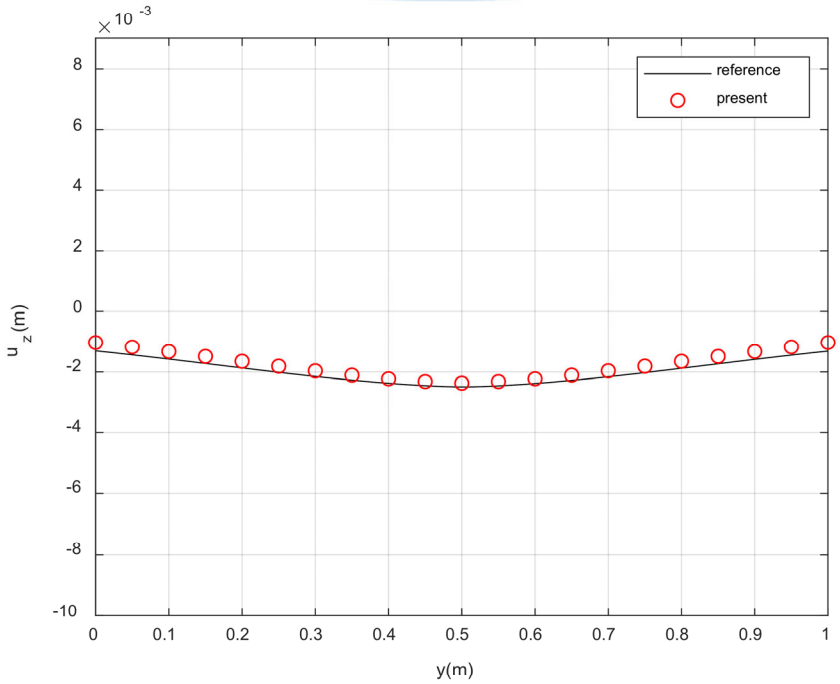

Fig. 4.15. Deflection in straight AB of shallow composite panel

Chapter 5. Conclusion

The purpose of this topic is to develop an element suitable for analyzing thin layered models in which partial interactions exist. Solid elements are currently used to analyze the slip, but there is a disadvantage that an extremely large number of elements must be used for accuracy when analyzing a very thin model.

In this study, a multi-layer composite shell element based on a continuum mechanics with interlayer slip was proposed. By defining two slip direction vectors per node, two degrees of freedom per node are added each time a layer is increased. Various numerical examples were presented to confirm the performance of the proposed element. First, a two-layer cantilever was compared with a reference model under various load conditions, and this was extended to a three-layer cantilever. In addition, an example of a cylinder with curvature and an example of a thin composite panel subjected to a centralized load were examined. All of the above example showed good accuracy when compared to reference model in ADINA.

When analyzing the proposed shell element thin composite structure, there is an advantage that the analysis can be performed using fewer degrees of freedom than using a shell element for each layer or using a solid element. It is also significant that the shell finite element analysis considering slip was performed using three-dimensional interpolation.

The current model only considers constant slip stiffness. For a mode II and III delamination analysis, a cohesive model in which the stiffness modulus changes with displacement is required. If expansion into nonlinear formulation is also considered, a more accurate analysis will be possible.

Bibliography

[1] Reissner, E, Stavsky, Y. Bending and stretching of certain type of heterogeneous elastic plates. Journal of Applied Mechanics 1961;9:402-408.

[2] Yang, P.C., Norris, C.H. and Stavsky, Y. Elastic Wave propagation in hetereogenous plates. International Journal of Solids and Structures 1966;2;665-684.

[3] A. Toledano, H. murakami. Shear-deformable two-layer plate theory with interlayer slip. Journal of Engineering Mechanics 1988;114(4):604-623.

[4] Marco Di Sciuva. Geometrically Nonlinear theory of multilayered plates with interlayer slip. AIAA J 1997;35(11):1753-1755.

[5] Newmark NM, Siess CP, Viest IM. Tests and analysis of composite beam with incomplete interaction. Proc Soc Exp Stress Anal 1951;9:75–92.

[6] Xu R, Wu YF. Static, dynamic and buckling analysis of partial interaction composite beams using Timoshenko's beam theory. Int J Mech Sci 2007;49: 1139–55.

[7] Ranzi G, Bradford MA, Uy B. A direct stiffness analysis of a composite beam with partial interaction. Int J Numer Methods Eng 2004;61:657–72.

[8] Hyo-Jin Kim, Kyungho Yoon. Continuum mechanics based beam elements for linear and nonlinear analysis of multi-layered composite beams with interlayer slips. Composite Structures 2020;235;111740.

[9] Suresh Panda, R. Natarajan, Analysis of laminated composite shell structures by finite element method 1981;14;225-230.

[10] K.J. Bathe, Finite element procedures, 2nd ed., K.J. Bathe, Watertown, (MA): KJ Bathe; 2014.

[11] E.N. Dvorking and K.J. Bathe, A continuum mechanics based four-node shell element for general nonlinear analysis. Engineering Computations 1984;1(1);77-88.